Atomic layer deposition of zinc sulfide with $Zn(TMHD)_2$

Andrew Short, Leila Jewell, Sage Doshay, Carena Church, Trevor Keiber, Frank Bridges, Sue Carter, and Glenn Alers[a)]
Department of Physics, University of California at Santa Cruz, 1156 High Street, Santa Cruz, California 95064

(Received 1 August 2012; accepted 20 November 2012; published 10 December 2012)

The atomic layer deposition (ALD) of ZnS films with $Zn(TMHD)_2$ and *in situ* generated H_2S as precursors was investigated, over a temperature range of 150–375 °C. ALD behavior was confirmed by investigation of growth behavior and saturation curves. The properties of the films were studied with atomic force microscopy, scanning electron microscopy, energy-dispersive x-ray spectroscopy, ultraviolet–visible–infrared spectroscopy, and extended x-ray absorption fine structure. The results demonstrate a film that can penetrate a porous matrix, with a local Zn structure of bulk ZnS, and a band gap between 3.5 and 3.6 eV. The ZnS film was used as a buffer layer in nanostructured PbS quantum dot solar cell devices. © *2013 American Vacuum Society*. [http://dx.doi.org/10.1116/1.4769862]

I. INTRODUCTION

Photovoltaics with absorber layers comprised of non-silicon material continue to be an expanding area of solar cell research. Often, in these devices, a buffer layer of cadmium sulfide (CdS) is used as an n type layer and to prevent shunting.[1] Recently, zinc sulfide (ZnS) has been substituted for the CdS, as its higher band gap should allow for greater efficiencies at shorter wavelengths by letting more high-energy photons through to the absorbing layer. Zinc is also more abundant than cadmium and is non-toxic. Atomic layer deposition (ALD) is the preferred method for creating this window layer, as it is a conformal process that operates at relatively low (~100 °C) temperatures, allows for deposition into highly structured substrates, and has a low energy cost.[2,3] Thus, ALD is an ideal method for creating a thin, highly conformal layer of material at low energy cost, such as a window layer of ZnS.

Previously, work in this field has focused on efforts with the precursors diethyl and dimethyl zinc (DEZn and DMZn).[3–7] These precursors have low boiling points (124 °C for DEZn and 46 °C for DMZn) and high vapor pressures, which make them excellent candidates for ALD. However, they are also pyrophoric and difficult to work with, each having a flash point of −18 °C. Therefore, an alternative precursor was considered for ALD of ZnS.

The precursor chosen was bis(2,2,6,6-tetramethyl-3, 5-heptanedionato)zinc ($Zn(TMHD)_2$), because it is a non-pyrophoric solid precursor used for the chemical vapor deposition of zinc sulfide.[8] The objective of this research was to examine the viability of $Zn(TMHD)_2$ as a precursor for atomic layer deposition, and to discover the ideal parameters for such a process.

II. EXPERIMENT

ALD growth of ZnS was performed in a custom-built hot wall tube furnace reactor. The base pressure of the system was 20 mTorr. Two precursors can be simultaneously introduced into the reactor chamber through separate injectors. Nitrogen was used as the carrier and purge gas at a constant flow rate of 40 sccm. Operating pressure was kept below 2 Torr during pulse and purge cycles.

The precursors used were $Zn(TMHD)_2$ and H_2S. $Zn(TMHD)_2$ is a solid powder at room temperature with a melting point of 144 °C and a boiling point of 250 °C at atmospheric pressure. The $Zn(TMHD)_2$ ampule was heated to 120 °C and all gas lines were heated to above 90 °C. The H_2S was created *in situ* via a reaction between aluminum sulfide powder and water, via the chemical reaction $Al_2S_3 + 3H_2O \rightarrow Al_2O_3 + 3H_2S$. Approximately, 2.5 g of Al_2S_3 powder was combined with 30 cc of water for each deposition. After the reaction was completed, the H_2S ampule was backfilled with N_2, resulting in a partial pressure for H_2S of ~400 mm Hg, and a total pressure in the ampule equal to ~750 mm Hg. The H_2S gas was passed through a powder desiccant to reduce the residual water content to less than 1% of the H_2S measured with a residual gas analyzer. If water were present in the hydrogen sulfide, there is a concern that ZnO might form instead of ZnS. However, the reaction $ZnO + H_2S \rightarrow ZnS + H_2O$ is exothermic with an enthalpy of −77 kJ/mol.[9,10] Therefore, any ZnO that forms would be converted to ZnS by the hydrogen sulfide.

The substrates used were 1 mm thick, 1 $in.^2$ quartz glass. The substrates were cleaned via a 30 min sonication in ethanol, and then dried with pressurized nitrogen. Resulting film thicknesses, morphology, and roughness were measured using an atomic force microscope (AFM) in tapping mode. Thickness was measured by abrasively removing a portion of the film and measuring the step height of remaining film. Stoichiometry was analyzed by energy-dispersive x-ray (EDX) spectroscopy using ZnS powder as a reference. Cross-sectional scanning electron microscopy (SEM) images of the film in a porous TiO_2 matrix were taken to observe the conformal coating of depositions. Structure was analyzed with extended x-ray absorption fine structure (EXAFS) measurements, described in detail below. Band gaps were determined by ultraviolet–visible–infrared spectroscopy (UV–Vis–IR), as discussed below. Solar cell devices were

a)Electronic mail: galers@ucsc.edu

made using the method described elsewhere.[11] Quartz substrates with patterned ITO were used with ~100 nm of sol–gel deposited TiO_2 and ~200 nm of 30 nm TiO_2 nanoparticles as the n type contact layer. A 2.5 nm layer of ALD ZnS was then deposited on top of the porous TiO_2 as a buffer layer. A 945 nm layer of PbS quantum dots was deposited using a ligand exchange method described elsewhere,[11] and finally a gold contact was deposited by evaporation. These devices were used to observe the effect of the ZnS as a buffer layer in a solar cell.

III. RESULTS AND DISCUSSION

A. Growth rate versus pulse times and temperature

ZnS growth rates as a function of precursor dose time and nitrogen purge time were studied with the substrate at 375 °C, and growth rate versus dose time was also studied at 150 °C. Growth rate was measured by dividing the film thickness (measured as a step edge by AFM) by the number of cycles. In Fig. 1, it is observed that longer dose times correspond to increased thickness per cycle at 375 °C indicating that some precursor decomposition is present at this temperature. However, for the lower temperatures this increase is proportionally smaller. For example, the percent increase in growth rate from a 1 s dose time to 10 s at 375 °C is 163%, while at 150 °C, the percent increase over the same range is only 50%. A purge time of approximately 25 s was required to prevent an increased growth rate characteristic of chemical vapor deposition, which is seen at shorter purge times as shown in Fig. 2. Therefore, the pulse sequence chosen for other depositions was a 2 s $Zn(TMHD)_2$ pulse, 25 s purge, 5 s H_2S pulse, and 25 s purge with a background nitrogen flow rate of 40 sccm. These parameters were used to analyze the behavior of the ZnS deposition process over the temperature range of 150–375 °C.

The growth rate was observed to decrease throughout this temperature range as shown in Fig. 3. This contrasts with chemical vapor deposition, where the growth rate increases with temperature, and is indicative of a surface limited ALD reaction for these films. The decrease in growth rate arises from surface desorption of the precursors at higher temperatures. The thicknesses of 150 and 375 °C films after 300 cycles were 51 and 15 nm, respectively, measured with an atomic force microscope, and correspond to growth rates of 1.7 and 0.5 Å/cycle. These rates are comparable to those in literature studies using DEZn and compressed H_2S gas. For example, the growth rate of 0.5 Å/cycle at 375 °C measured in this study is similar to the 0.7 Å/cycle growth rate at 300 °C determined by Kim and Yun.[4] Also, Platzer-Bjorkman *et al.*[5] observed a growth rate of 1.38 Å/cycle at 120 °C on glass which is comparable to this work's measured value of 1.7 Å/cycle at 150 °C. Using the ZnS lattice dimension of 3.13 Å for c(111), these growth rates range from 0.54 monolayers/cycle at 150 °C to 0.16 monolayers/cycle at 375 °C.

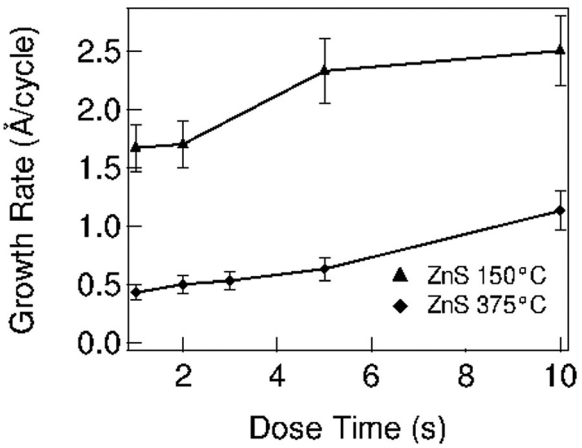

FIG. 1. ZnS growth rate vs $Zn(TMHD)_2$ dose time at 375 and 150 °C, showing that with more precursor time, the growth rate increases, demonstrating decomposition, which is reduced at the lower temperature.

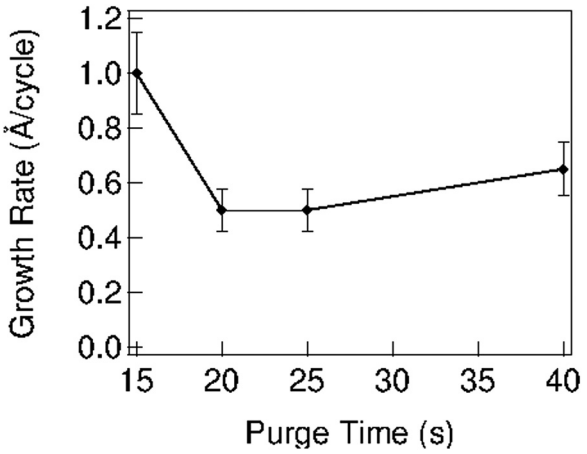

FIG. 2. Growth rate vs nitrogen purge time at 375 °C. Longer purge times prevent CVD behavior, which can be seen for purges as long as 15 s.

B. Photospectroscopy

Optical characterization of the films was performed with UV–Vis–IR for determination of the band gap. ZnS is a direct band gap semiconductor, with a band gap for films and nanoparticles reported in the literature of 3.5–4.1 eV.[12–19]

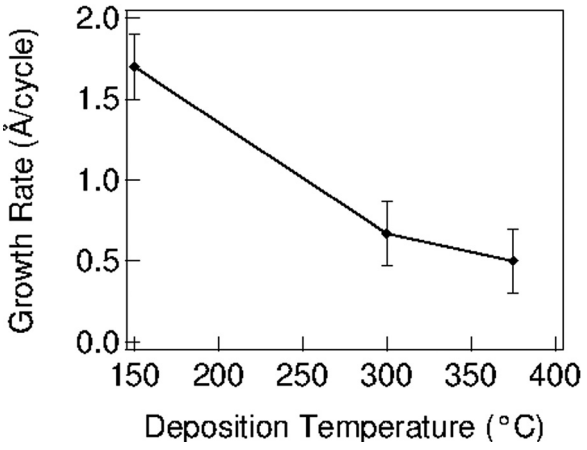

FIG. 3. Growth rate vs temperature. The decreased growth rate at higher temperatures is the opposite of expected CVD behavior, where film growth increases with temperature. The observed behavior corresponds to decreased surface adhesion of the precursors with increased substrate temperature.

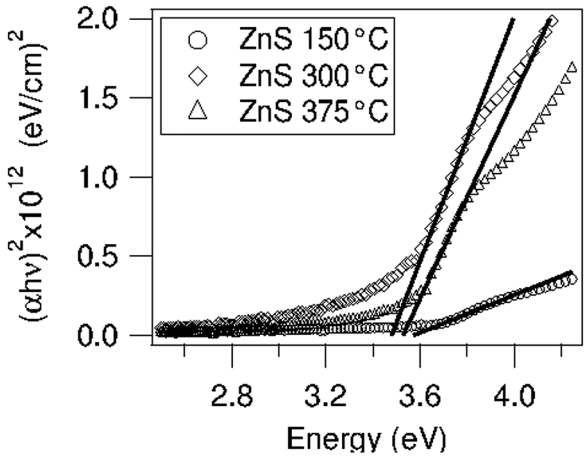

FIG. 4. Three Tauc plots, showing the band gap of deposited ZnS is relatively constant with temperature and approximately 3.5 eV.

Most reports remark that for cubic ZnS the band gap is 3.68 eV and for hexagonal ZnS it is 3.74–3.87.[20] UV–Vis–IR was performed on 300 cycle films deposited at temperatures of 150, 300, and 375 °C, and selected results are shown in Fig. 4. Tauc plots of $(\alpha h\nu)^2$ versus $h\nu$ were used to estimate the band gap for the films.[21] Films at all three temperatures display a band gap between 3.47 and 3.58 eV, at the low end of accepted values for cubic ZnS. The lower range may be due to band broadening from increased disorder in the films.

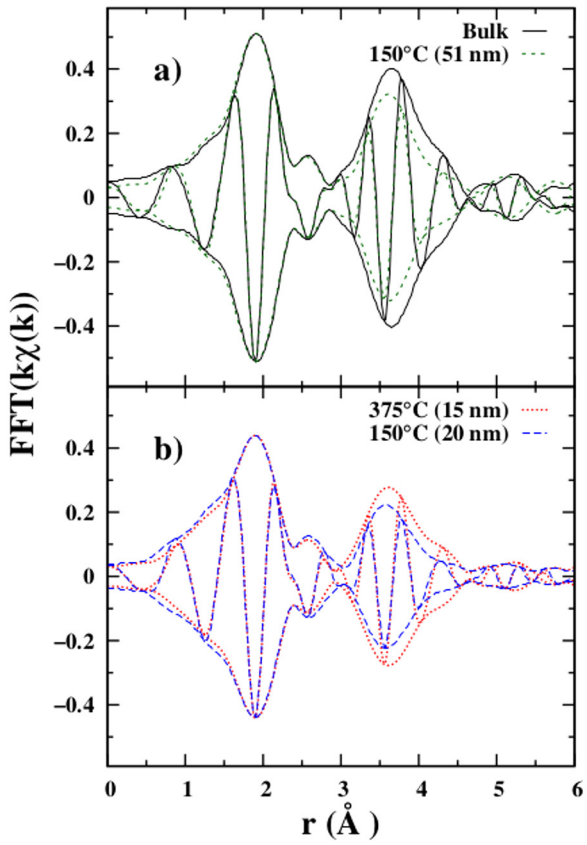

FIG. 5. (Color online) EXAFS data comparing (a) thin film ZnS to bulk and (b) films of comparable thickness deposited at different temperatures. The significantly smaller second peak amplitude (Zn-Zn) indicates increased disorder as the film thickness decreases.

This disorder could arise from the presence of both cubic and hexagonal ZnS.[22] This conclusion also agrees with a previous report by Lahtinen *et al.*, using electroreflectance to show that both cubic and hexagonal phases are present in ALD ZnS films grown at certain temperatures.[23] Studies in the literature have claimed that the hexagonal phase becomes the dominant phase in the 400–500 °C range.[4,24]

C. Composition and structure via EDX and EXAFS

The stoichiometric composition of our films was determined via EDX measurements. The measured percent weights of the sulfur and zinc in each sample were converted to a stoichiometric ratio by comparison with the measured percent weights of the same elements in a control sample of pure ZnS powder. As seen in Table I, our films are within 6% of 1:1 stoichiometric ZnS. The EXAFS data were collected at the Stanford Synchrotron Radiation Lightsource (SSRL) on beamline 4-1 using a Si (220) double monochromator, detuned 50% at 9800 eV to reduce harmonics. The Zn K-edge data were collected in fluorescence mode with a Ge multichannel detector at a temperature of 8 K. Slit heights were approximately 0.5 mm, which give an energy resolution of ~0.9 eV. The data were reduced using standard techniques (RSXAP),[25] converted to k-space, and Fourier transformed into r-space. The Fourier transform range for all the samples is 3.5–10.5 $Å^{-1}$. The Zn K-edge data for a 51 nm thin film of ZnS deposited at 150 °C, a 20 nm film deposited at 150 °C, and a 15 nm film deposited at 375 °C were compared with control samples of bulk ZnS. The first peak (Zn-S) corresponds to the nearest S neighbors, while the second peak (Zn-Zn) corresponds to the next neighbors, Zn. It is clear from Fig. 5 that the thin film data are very similar to that for the bulk material; the main difference is a reduced amplitude, particularly for the second peak. This second peak reduction is indicative of either increased local disorder in the film or smaller nanoscale grain sizes in the film. The first peak for the 51 nm film and bulk ZnS has the same amplitude, whereas the other two thin films have a slight reduction in this peak, indicating more disorder for the nearest neighbors. For films as thin as these two, the effects of the substrate and/or increased disorder are seen for all peaks. In addition, the data show that the relative disorder in the films increases with decreasing film thickness as well as with decreasing temperature. However, the reduced peak amplitude at 3.5 Å for the 150 °C film may indicate that the lower temperature deposition correlates to smaller grain size formation than for the higher temperature films.

TABLE I. Electron dispersive x-ray spectroscopy data comparing the percent weights of sulfur and zinc in deposited films with those for a bulk control. Using this control, the stoichiometric ratio of Zn:S for each sample was determined.

	Control	ZnS 150 °C	ZnS 300 °C	ZnS 375 °C
Sulfur (wt. %)	38.9	22.83	16.57	13.8
Zinc (wt. %)	23.93	14.95	9.93	9.03
Stoichiometric ratio (Zn:S)	1:1	1.06:1	0.97:1	1.06:1

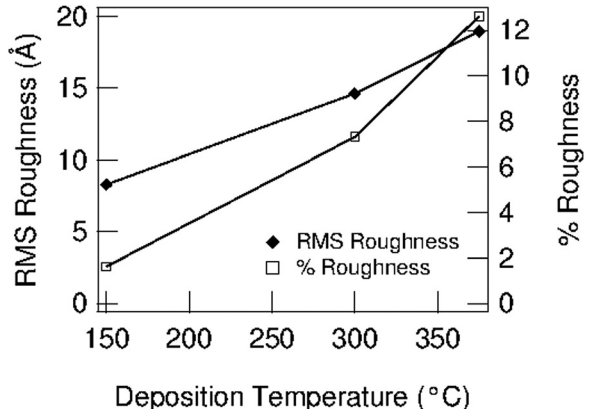

FIG. 6. RMS roughness and % roughness determined via AFM as a function of deposition temperature for 300 cycle ZnS films deposited.

D. Surface roughness and interpenetration of ALD ZnS

Film roughness was studied for a series of films deposited at 375, 300, and 150 °C. The RMS roughness as determined by AFM as well as the percent roughness is plotted in Fig. 6 as a function of deposition temperature. It can be seen that the roughness increases with deposition temperature as the overall film thickness falls (see Fig. 3), causing the percent roughness to vary from 1.62% at 150 °C to 12.62% at 375 °C. As shown from the EXAFS results, the high deposition temperatures may correspond to larger grains, which in a thinner film would result in higher roughness.

Film roughness as a function of thickness was studied for a series of films deposited at 150 °C. These data are plotted in Fig. 7 as a function of film thickness. It can be seen that the roughness increases with thickness, and the percent roughness decreases over the same range from 3.11% for 200 Å thick films to 1.62% for 510 Å thick films. This compares favorably with data published by Bakke *et al.*[22] as well as Kim and Yun,[4] which show a similar overall roughness increase with thickness, while the percent roughness falls.

The interpenetrating nature of ALD was verified for this material via cross-sectional SEM imaging, using a nanoporous TiO_2 substrate imaged both with and without deposited

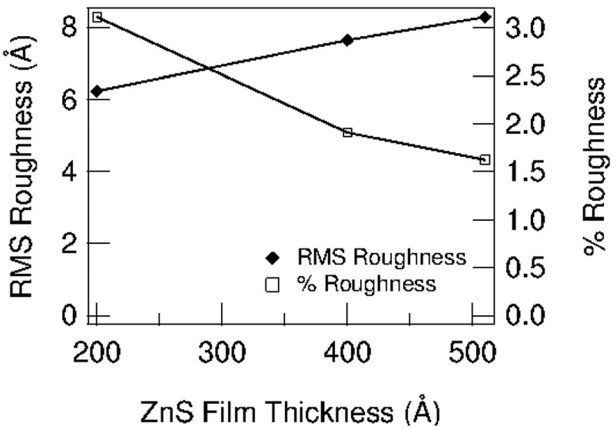

FIG. 7. RMS roughness and % roughness determined via AFM as a function of film thickness for films deposited at 150 °C.

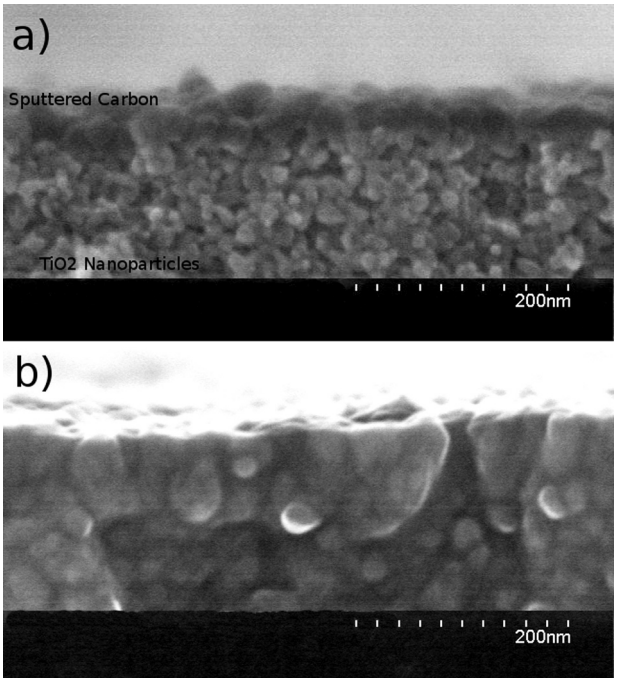

FIG. 8. Cross-sectional SEM images of TiO_2 nanoparticles, with (a) no ZnS film, but a sputtered layer of carbon to prevent charging during imaging, and (b) a ZnS film deposited via ALD at 150 °C.

ZnS. With ALD, there is expected to be a highly conformal coating of the porous substrate. The images show this coating of the nanoparticles within the nanoporous structure as a reduction in the number of voids and bridging between the nanoparticles, as the deposited film fills in the voids in the TiO_2 matrix. This can be seen in Fig. 8, observing in the upper image the nanograins of TiO_2 and in the lower image the coating of the TiO_2 by the ZnS.

E. Solar cell device data

Lead sulfide quantum dot devices with and without a 2.5 nm ZnS buffer layer were measured under a 1 sun, AM

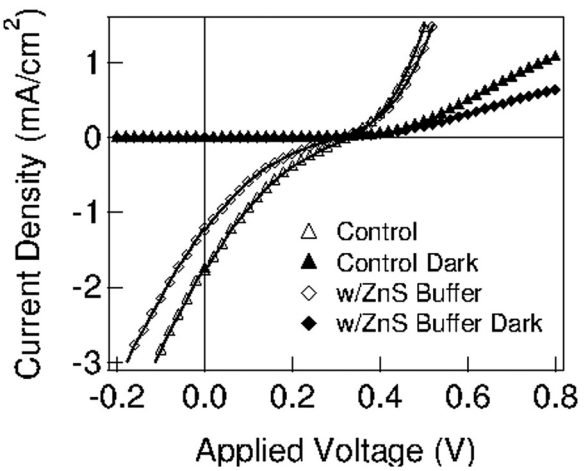

FIG. 9. J–V light and dark curves for the most efficient control device with no ZnS layer and for the most efficient device with a 2.5 nm ZnS buffer layer between a nanoporous TiO_2 layer and PbS quantum dot absorbers. The control device has an efficiency of 0.098%, while the efficiency of the device with ZnS is 0.06%.

1.5 light source (dark curves were also taken), measuring short circuit current, open circuit voltage, fill factor, and overall power conversion efficiency. The device stack was quartz/ITO/sol–gel TiO_2/nanoparticle TiO_2/(ZnS)/nanoparticle PbS/Au. Each sample consisted of six 1×3 mm^2 devices that were all functional. The J–V curves for the device of each kind with the highest efficiency are plotted in Fig. 9. The best device with no ZnS has a J_{sc} of 1.79 mA, a V_{oc} of 0.33 V, and a fill factor of 0.165, which results in a power conversion efficiency of 0.098%. This can be compared with the highest efficiency device that included a 2.5 nm ZnS buffer layer. The ZnS device has a J_{sc} of 1.25 mA, a V_{oc} of 0.31 V, and a fill factor of 0.155, which results in a power conversion efficiency of 0.06%. Despite the reduction of overall efficiency in the device with the ZnS layer, there is only a very small reduction in V_{oc} indicating that the band alignment is not affected by the ZnS layer. The data show that the J_{sc} in devices with the ZnS layer drops by almost a third, indicating poor charge transport in the devices that contain ZnS. This may be due to an increase in series resistance caused by the insulating ZnS layer.

IV. SUMMARY AND CONCLUSIONS

ZnS ALD using $Zn(TMHD)_2$ and *in situ* generated H_2S has been demonstrated. The growth behavior of the films follows expected ALD behavior. Complete surface saturation with increased dose time was not readily observed due to precursor decomposition. Growth rates were comparable to those in the literature for ALD of ZnS with traditional precursors. The ALD temperature dependence was investigated from 150 to 375 °C, and the growth rate was found to decrease over that temperature range in contrast to CVD behavior. The band gap obtained from Tauc plots was 3.5–3.6 eV, slightly lower than the reported literature values. The lower band gap may be from disorder-induced band broadening, as increased disorder of the films relative to bulk ZnS was seen in EXAFS. The EXAFS data also indicate that this disorder increases at lower growth temperatures and at reduced film thicknesses, and that the grain size of the grown ZnS likely increases with temperature. The surface roughness was demonstrated to be a function of deposition temperature, and the depositions at the ideal parameters were observed to penetrate within a porous matrix. Finally, devices with a buffer layer of ZnS were studied, showing little decrease in V_{oc} despite a somewhat large drop in J_{sc}. The device results demonstrate that the ZnS layer is acting as a highly resistive layer between the PbS and the TiO_2 with no impact on band alignment.

ACKNOWLEDGMENTS

This work was supported by the National Science Foundation (Grant No. DMR-1006190). The SEM and EDX measurements were conducted at the MACS center at NASA Ames. The EXAFS experiments were carried out at the Stanford Synchrotron Radiation Lightsource, operated by the DOE, Division of Chemical Sciences. The authors thank Allison Breeze of Solexant for supplying the PbS nanoparticles.

[1]T. Nakada, M. Mizutani, Y. Hagiwara, and A. Kunioka, Sol. Energy Mater. Sol. Cells **67**, 255 (2001).
[2]S. M. George, Chem. Rev. **110**, 111 (2010).
[3]J. Maula, Chin. Opt. Lett. **8**, 53 (2010).
[4]Y. S. Kim and S. J. Yun, Appl. Surf. Sci. **229**, 105 (2004).
[5]C. Platzer-Bjorkman, T. Torndahl, D. Abou-Ras, J. Malmstrom, J. Kessler, and L. Stolt, J. Appl. Phys. **100**, 044506 (2006).
[6]G. Stuyven, P. De Visschere, A. Hikavyy, and K. Neyts, J. Cryst. Growth **234**, 690 (2002).
[7]J. T. Tanskanen, J. R. Bakke, T. A. Pakkanen, and S. F. Bent, J. Vac. Sci. Technol. A **29**, 031507 (2011).
[8]L. V. Saraf, M. H. Engelhard, C. M. Wang, A. S. Lea, D. E. McCready, V. Shutthanandan, D. R. Baer, and S. A. Chambers, J. Mater. Res. **22**, 1230 (2007).
[9]J. D. Cox, D. D. Wagman, and V. A. Medvedev, *CODATA Key Values for Thermodynamics* (Hemisphere, New York, 1984).
[10]S. Deore and A. Navrotsky, Am. Mineral. **91**, 400 (2006).
[11]G. M. Zhai, A. Bezryadina, A. J. Breeze, D. L. Zhang, G. B. Alers, and S. A. Carter, Appl. Phys. Lett. **99**, 063512 (2011).
[12]R. G. Zhang, B. Y. Wang, and L. Wei, Vacuum **82**, 1208 (2008).
[13]P. Prathap, N. Revathi, Y. P. V. Subbaiah, and K. T. R. Reddy, J. Phys.: Condens. Matter **20**, 035205 (2008).
[14]K. R. Murali, S. Vasantha, and K. Rajamma, Mater. Lett. **62**, 1823 (2008).
[15]Q. Liu and G. B. Mao, Surf. Rev. Lett. **16**, 469 (2009).
[16]F. Gode, C. Gumus, and M. Zor, J. Cryst. Growth **299**, 136 (2007).
[17]K. S. Rathore, D. Patidara, Y. Janu, N. S. Saxena, K. Sharma, and T. P. Sharma, Chalcogenide Lett. **5**, 105 (2008).
[18]K. Sreejith, K. S. Mali, and C. G. S. Pillai, Mater. Lett. **62**, 95 (2008).
[19]J. P. Borah and K. C. Sarma, Acta Phys. Pol. A **114**, 713 (2008).
[20]O. L. Arenas, M. T. S. Nair, and P. K. Nair, Semicond. Sci. Technol. **12**, 1323 (1997).
[21]Z. Chen *et al.*, J. Mater. Res. **25**, 3 (2010).
[22]J. R. Bakke, J. S. King, H. J. Jung, R. Sinclair, and S. F. Bent, Thin Solid Films **518**, 5400 (2010).
[23]J. A. Lahtinen, A. Lu, T. Tuomi, and M. Tammenmaa, J. Appl. Phys. **58**, 1851 (1985).
[24]J. Ihanus, M. Ritala, M. Leskelä, T. Prohaska, R. Resch, G. Friedbacher, and M. Grasserbauer, Appl. Surf. Sci. **120**, 43 (1997).
[25]C. H. Booth, R-Space X-ray Absorption Package, 2010, see http://lise.lbl.gov/RSXAP/.